Extended PVFC with Variable Velocity Fields for Kneed Biped

Fumihiko Asano[1] and Masaki Yamakita[2]

[1] Department of Control Engineering, Tokyo Institute of Technology,
2-12-1 Oh-okayama, Meguro-ku, Tokyo 152-8552, JAPAN
E-mail: asano@ctrl.titech.ac.jp
[2] Department of Control and Systems Engineering, Tokyo Institute of Technology,
2-12-1 Oh-okayama, Meguro-ku, Tokyo 152-8552, JAPAN
E-mail: yamakita@ctrl.titech.ac.jp

Abstract. In this paper, two aspects for the task specification and control of biped walking robot:

1. Realization of safe control against human-being and outside-environment by utilizing passive velocity field controller.
2. Energy-effective gait design based on virtual passive dynamic walking.

are studied and a new control method is derived based on them. In our previous work, we have given a method which satisfied the required properties and examined by numerical simulations. In the method single trajectory is realized, however, the walking behavior should be modified and adapted by its energy-level and initial conditions. Based on the observation, we introduce multi-pattern walking of virtual passive gait to realize more natural walking motion The virtual passive walking has been checked to require less control input than other method which can generate a limit cycle automatically without any gait design and we should combine virtual passive walk with PVFC to change its walking speed easily and effectively.

1 Introduction

The study of bipedal walking in the framework of humanoid robot is resent active research area. The gait design problem is most important part of legged robot control, however, most of them imitate human gait intuitively without any solid reason which ensure some optimality, especially energy-consumptions. Based on the observation, in this paper we will focus on "passive dynamic walking" originally studied by McGeer.[8] The model of walking robot is designed based on a passive walker which is designed by McGeer[8] and numerically studied by INRIA[5][6][7] and Garcia et. al.[9][10] McGeer designed several unpowered biped robots and studied their gravity-induced passive motion on gentle slopes. He demonstrated that the prototype can attain a stable steady periodic motion and analyzed this behavior with a linearized mathematical model. Furthermore, INRIA studied such a passive system by means of its full nonlinear equations and verified the symmetric and chaotic motion. We extended their compass-like biped robot to a kneed robot which also exhibits passive walk on a gentle slope. The passive motion has a special feature because it is *natural* because it does not require any external energy source except gravity effect. It is clear that the human gait depends on the geometry and internal properties of human body. Since human can walk a long distance with small energy supply, the gait takes advantage of the gravity effect as "passive" walk. On the level ground, however, the robot cannot walk without any control forces. Then we introduce "virtual gravity field"[11][12] toward the horizontal direction which acts as a driving force for walking robots. In this case, the robot is also able to realize virtual passive walking on the level ground by a virtual gravity field, and we use its steady gait as a desired trajectory of the walking robot which walks on the level ground by actuators.

On the other hand, the desired trajectory has usually been time-dependent so the controller sometimes generates very large force to catch up with its desired one even if there exists obstacles, human-being and so on. The safety of control system has not been guaranteed in that case. The PVFC controller mimics an augmented system which consists of the original system and a flywheel: the flywheel stores and releases energy to the walking robot, but does not generate any. [1][2](Fig. 1) As we applied a decentralized PVFC to cooperative multi-manipulators systems and cooperative mobile robot systems[3][4], in this paper, we apply PVFC to the control of biped walking robot which walks on the level ground by actuators. The idea of application of PVFC to walking robots has been mentioned in the original paper by Li[2], however, any concrete algorithm has not been studied. In our approach we combine the PVFC with the virtual passive walker on the level ground which generates automatically an effective energy dependent walking pattern utilizing only virtual gravity effect by multi velocity fields. A method to compensate for energy losses at walking phases due to collisions to the floor is also proposed.

According to above methods, energy-effective and safety control for biped walking robot on the level ground can be obtained because of passivity of the control system. The validity of the proposed method is demonstrated by numerical simulations.

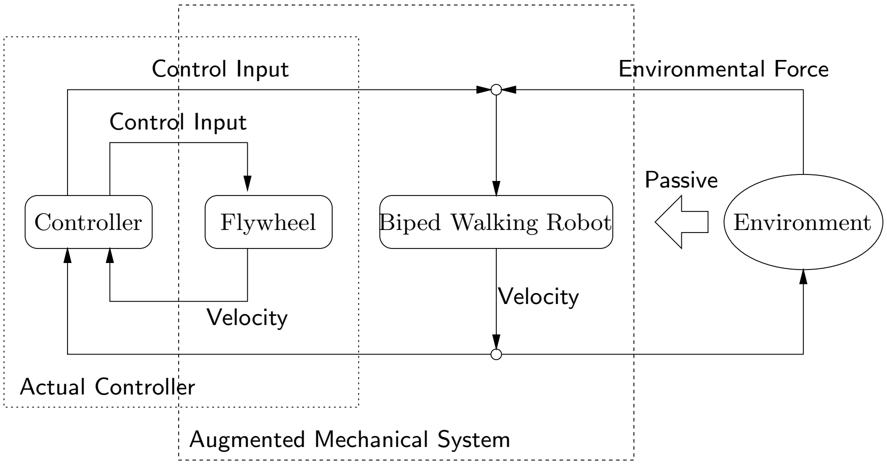

Fig. 1. Passive Velocity Field Control

2 Modeling and Virtual Passive Walking

2.1 Model assumptions and parameter settings

Fig. 2 shows a model of the walking robot. The robot cannot walk without any control forces on the level ground. Then let us consider "virtual gravity field" toward the horizontal direction. With it, the robot can exhibit passive walking virtually on the level ground utilizing only virtual gravity effect. If $\phi = 0.05$ [rad], the walking motion converges 1-periodic stable limit cycle. The condition means that the robot seems to be on a gentle slope ϕ in the nominal gravity field whose magnitude is $g/\cos\phi$.

The modeling assumptions are listed as follows:

1. *Mass*: concentrated at 4 points. (hip, stance leg, thigh and shank)
2. *Actuation*: full-control, i.e., a rotational actuators is assumed to be implemented at each joint as well as the contact point. In the case of virtual passive walk, the robot is un-actuated and $\phi = 0.0$ [rad].
3. *Knee-joint*: kept straight (locked) after knee-strike. The robot can be regarded as compass-like 2-link robot after knee-lock and heel-strike instant.
4. *Collision (heel-strike)*: the impact of the swing leg with the ground is assumed to be inelastic and without sliding.

We can see that the knee-joint is locked and kept straight after knee-strike. (Fig. 3) Then the robot can be regarded as the compass-like biped robot at heel-strike collision, so the heel-strike transition equation can be applied to the kneed robot directly.

2.2 Equations of the robot

We use the gait pattern by the virtual gravity field as a desired trajectory of the walking robot which walks on a level by actuators. In this paper, we set $\phi = 0.05$ [rad]. Since the value of ϕ is very small, this condition can be considered to be very closed to real condition, so the gait pattern can be considered to be *natural.*

The dynamic equation of the robot without constraints considered later is obtained by well-known Euler-Lagrange approach as

$$\frac{d}{dt}\left(\frac{\partial \mathcal{L}(\boldsymbol{\theta}, \dot{\boldsymbol{\theta}}, \phi)}{\partial \dot{\theta}_i}\right) - \frac{\partial \mathcal{L}(\boldsymbol{\theta}, \dot{\boldsymbol{\theta}}, \phi)}{\partial \theta_i} = \tau_i + \tau_{ei} \quad (i = 1, 2, 3) \tag{1}$$

where the Lagrangian $\mathcal{L}(\boldsymbol{\theta}, \dot{\boldsymbol{\theta}}, \phi)$ is the difference between the kinetic energy and the potential energy of the robot, that is, $\mathcal{L}(\boldsymbol{\theta}, \dot{\boldsymbol{\theta}}, \phi) = K(\boldsymbol{\theta}, \dot{\boldsymbol{\theta}}) - P(\boldsymbol{\theta}, \phi)$. K is kinetic energy and P is potential energy of the robot. $\boldsymbol{\theta} = \begin{bmatrix}\theta_1 \ \theta_2 \ \theta_3\end{bmatrix}^T$ is configuration of the robot. The dynamic equation is given by

$$\boldsymbol{M}(\boldsymbol{\theta})\ddot{\boldsymbol{\theta}} + \boldsymbol{h}(\boldsymbol{\theta}, \dot{\boldsymbol{\theta}}, \phi) = -\boldsymbol{J}_r^T \lambda_r + \boldsymbol{\tau} + \boldsymbol{\tau}_e \tag{2}$$

where $\boldsymbol{M}(\boldsymbol{\theta}) = [3 \times 3]$ is the inertia matrix and $\boldsymbol{h}(\boldsymbol{\theta}, \dot{\boldsymbol{\theta}}, \phi) = [3 \times 1]$ is colioris and gravity term, that is:

$$\boldsymbol{h}(\boldsymbol{\theta}, \dot{\boldsymbol{\theta}}, \phi) = \boldsymbol{C}(\boldsymbol{\theta}, \dot{\boldsymbol{\theta}})\dot{\boldsymbol{\theta}} + \boldsymbol{g}(\boldsymbol{\theta}, \phi) \tag{3}$$

where $\boldsymbol{C}(\boldsymbol{\theta}, \dot{\boldsymbol{\theta}}) = [3 \times 3]$ and $\boldsymbol{g}(\boldsymbol{\theta}, \phi) = [3 \times 1]$. $\boldsymbol{J}_r^T \lambda_r$ is the constrained force at knee-joint. Before knee-lock, $\lambda_r = 0$. After knee-lock, λ_r is determined as explained later. Please notice that in the case of the real robot walking on the floor with control forces that $\phi = 0$. The details of the terms are as follows:

$$\boldsymbol{M}(\boldsymbol{\theta}) = \begin{bmatrix} m_1 a_1^2 + (m_H + m_2 + m_3) l_1^2 & -(m_2 b_2 l_1 + m_3 l_1 l_2)\cos(\theta_1 - \theta_2) & -m_3 b_3 l_1 \cos(\theta_1 - \theta_3) \\ -(m_2 b_2 l_1 + m_3 l_1 l_2)\cos(\theta_1 - \theta_2) & m_2 b_2^2 + m_3 l_2^2 & m_3 b_3 l_2 \cos(\theta_2 - \theta_3) \\ -m_3 b_3 l_1 \cos(\theta_1 - \theta_3) & m_3 b_3 l_2 \cos(\theta_2 - \theta_3) & m_3 b_3^2 \end{bmatrix} \tag{4}$$

$$\boldsymbol{C}(\boldsymbol{\theta}, \dot{\boldsymbol{\theta}}) = \begin{bmatrix} 0 & -(m_2 b_2 l_1 + m_3 l_1 l_2)\sin(\theta_1 - \theta_2)\dot{\theta}_2 & -m_3 b_3 l_1 \sin(\theta_1 - \theta_3)\dot{\theta}_3 \\ (m_2 b_2 l_1 + m_3 l_1 l_2)\sin(\theta_1 - \theta_2)\dot{\theta}_1 & 0 & m_3 b_3 l_2 \sin(\theta_2 - \theta_3)\dot{\theta}_3 \\ m_3 b_3 l_1 \sin(\theta_1 - \theta_3)\dot{\theta}_1 & -m_3 b_3 l_2 \sin(\theta_2 - \theta_3)\dot{\theta}_2 & 0 \end{bmatrix} \tag{5}$$

$$\boldsymbol{g}(\boldsymbol{\theta}, \phi) = \begin{bmatrix} -(m_1 a_1 + m_2 l_1 + m_3 l_1 + m_H l_1)\sin(\theta_1 + \phi) \\ (m_2 b_2 + m_3 l_2)\sin(\theta_2 + \phi) \\ m_3 b_3 \sin(\theta_3 + \phi) \end{bmatrix} \frac{g}{\cos\phi} \tag{6}$$

$$\boldsymbol{\tau} = \boldsymbol{S}\boldsymbol{u} = \begin{bmatrix} 1 & 1 & 0 \\ 0 & -1 & -1 \\ 0 & 0 & 1 \end{bmatrix} \begin{bmatrix} u_1 \\ u_2 \\ u_3 \end{bmatrix} \tag{7}$$

It can be easily shown that a algebraic transition equations relate the robot's states just before and just after its collision with the ground. The stance leg (Link1) and swing leg (Link2, 3) switch during transition. We assume that the robot can be regarded as 2-link robot at the impact, the transition equation is obtained as 2 dimensional equation. Then the pre-impact and the post-impact configurations of the robot can be simply expressed as $\boldsymbol{\theta}^+ = \boldsymbol{J}_1 \boldsymbol{\theta}_{(2)}^-$ where the index "$-$" means before collision, the index "+" means after collision. The relationship are given as follows:

$$\boldsymbol{\theta}^+ = \boldsymbol{J}_1 \boldsymbol{\theta}_{(2)}^- \tag{8}$$

$$\boldsymbol{J}_1 = \begin{bmatrix} 0 & 1 \\ 1 & 0 \\ 1 & 0 \end{bmatrix} \tag{9}$$

The subscript (2) means the coordinate of 2-link robot: $\boldsymbol{\theta}_{(2)} = \begin{bmatrix}\theta_1 \ \theta_3\end{bmatrix}^T$.

Table 1. Notations and numerical settings

Link 1	stance leg (knee-locked)		
Link 2	thigh (upper part of swing leg)		
Link 3	shank (lower part of swing leg)		
Hip	body part		
m_1	stance leg mass	5.00	kg
m_2	thigh mass	3.50	kg
m_3	shank mass	1.50	kg
m_H	hip mass	10.0	kg
M_f	mass of flywheel	10.0	kg
a_1	lower part of stance leg	0.53	m
a_2	lower part of thigh	0.15	m
a_3	lower part of shank	0.25	m
b_1	upper part of stance leg	0.47	m
b_2	upper part of thigh	0.35	m
b_3	upper part of shank	0.25	m
l_1	stance leg length	1.00	m
l_2	thigh length	0.50	m
l_3	shank length	0.50	m
g	gravity acceleration	9.81	m/sec^2
ϕ	virtual slope		rad
θ_1	stance leg angle w.r.t. vertical		rad
θ_2	thigh angle w.r.t. vertical		rad
θ_3	shank leg angle w.r.t. vertical		rad
u_1	angle torque		Nm
u_2	hip torque		Nm
u_3	knee torque		Nm

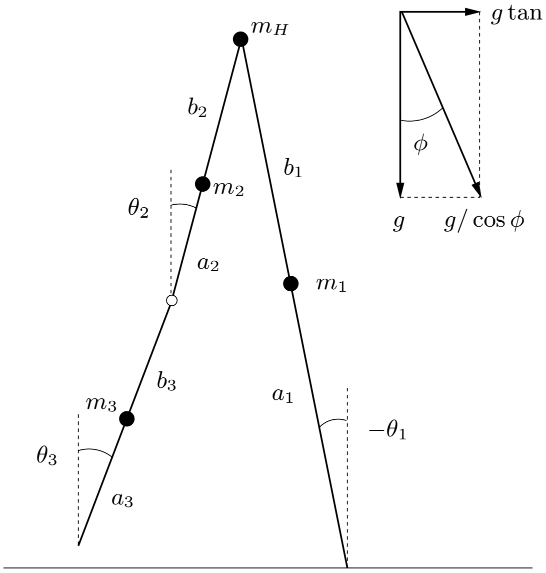

Fig. 2. Model of the robot and virtual gravity field

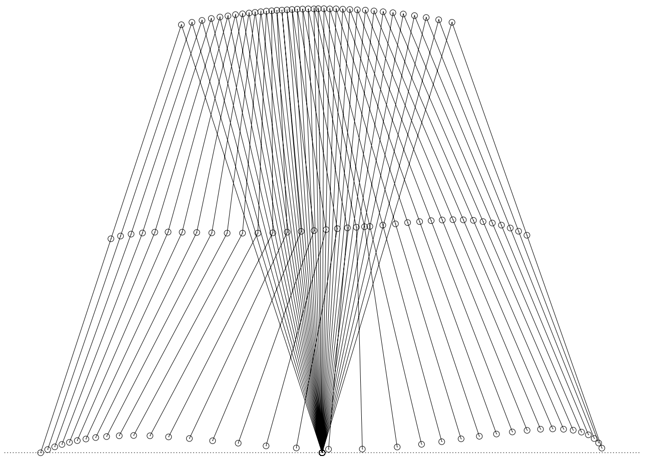

Fig. 3. Stick diagram

We assume that the angular momentum of the robot about the impacting foot as well as the angular momentum of the pre-impact support leg about the hip are conserved. With the above assumption, we obtain the following simple equation between the pre-impact and post-impact angular velocities

$$\boldsymbol{Q}^{+}(\alpha)\dot{\boldsymbol{\theta}}_{(2)}^{+} = \boldsymbol{Q}^{-}(\alpha)\dot{\boldsymbol{\theta}}_{(2)}^{-} \tag{10}$$

where

$$\boldsymbol{Q}^{+}(\alpha) = \begin{bmatrix} m_H l_1^2 + m_1 a_1^2 + m_1 l_1 (l_1 - b_1 \cos 2\alpha) & m_1 b_1 (b_1 - l_1 \cos 2\alpha) \\ -m_1 b_1 l_1 \cos 2\alpha & m_1 b_1^2 \end{bmatrix} \tag{11}$$

$$\boldsymbol{Q}^{-}(\alpha) = \begin{bmatrix} (m_H l_1^2 + 2 m_1 a_1 l_1) \cos 2\alpha - m_1 a_1 b_1 & -m_1 a_1 b_1 \\ -m_1 a_1 b_1 & 0 \end{bmatrix} \tag{12}$$

$$\alpha = \frac{\theta_1^- - \theta_3^-}{2} = \frac{\theta_3^+ - \theta_1^+}{2} > 0. \tag{13}$$

2.3 Knee-strike collision model

In this paper, we use extended INRIA's model which partially contains variable constraint. The constrained force is exerted only to knee-joint after knee-lock. The tip of stance leg is assumed to be always constrained to the ground.

The equation of knee-strike collision is given by

$$\boldsymbol{M}(\boldsymbol{\theta}^+)\dot{\boldsymbol{\theta}}^+ = \boldsymbol{M}(\boldsymbol{\theta}^-)\dot{\boldsymbol{\theta}}^- - \boldsymbol{J}_i^T \lambda_i \tag{14}$$

where λ_i is an effect of impulsive force. The constrained condition can be expressed by:

$$\boldsymbol{J}_i \dot{\boldsymbol{\theta}}^+ = 0. \tag{15}$$

Please notice that $\boldsymbol{M}(\boldsymbol{\theta}^+) = \boldsymbol{M}(\boldsymbol{\theta}^-) = \boldsymbol{M}(\boldsymbol{\theta})$ in Eq.(14) because of $\boldsymbol{\theta}^+ = \boldsymbol{\theta}^-$. From Eq.(14) we have

$$\dot{\boldsymbol{\theta}}^+ = \dot{\boldsymbol{\theta}}^- - \boldsymbol{M}(\boldsymbol{\theta})^{-1} \boldsymbol{J}_i^T \lambda_i. \tag{16}$$

From Eq.(15) and (16), the following relation is obtained:

$$\boldsymbol{J}_i \dot{\boldsymbol{\theta}}^+ = 0 = \boldsymbol{J}_i \dot{\boldsymbol{\theta}}^- - \boldsymbol{J}_i \boldsymbol{M}(\boldsymbol{\theta})^{-1} \boldsymbol{J}_i^T \lambda_i. \tag{17}$$

Therefore impulsive constrained force at knee-strike is given by

$$\lambda_i = X_i^{-1} \boldsymbol{J}_i \dot{\boldsymbol{\theta}}^- \tag{18}$$

where $X_i = \boldsymbol{J}_i \boldsymbol{M}(\boldsymbol{\theta})^{-1} \boldsymbol{J}_i^T$.

2.4 Knee-lock constrained force

The dynamic equation of the robot with constraint forces is given by

$$\boldsymbol{M}(\boldsymbol{\theta})\ddot{\boldsymbol{\theta}} + \boldsymbol{h}(\boldsymbol{\theta}, \dot{\boldsymbol{\theta}}, \phi) = -\boldsymbol{J}_r^T \lambda_r \tag{19}$$

The constrained condition at knee-joint is given by geometric relation: $\theta_2 = \theta_3$. By differentiating the condition w.r.t. time, we get $\dot{\theta}_2 = \dot{\theta}_3$. This can be rewritten in the form: $\boldsymbol{J}_r \dot{\boldsymbol{\theta}} = 0$ where $\boldsymbol{J}_r = \begin{bmatrix} 0 & -1 & 1 \end{bmatrix}$. Since the condition $\boldsymbol{J}_r \ddot{\boldsymbol{\theta}} = 0$ also holds, we get the following condition

$$\boldsymbol{J}_r \ddot{\boldsymbol{\theta}} = -\boldsymbol{J}_r \boldsymbol{M}(\boldsymbol{\theta})^{-1} \left(\boldsymbol{h}(\boldsymbol{\theta}, \dot{\boldsymbol{\theta}}, \phi) + \boldsymbol{J}_r^T \lambda_r \right) = 0. \tag{20}$$

Then the constrain force is given by

$$\lambda_r = -X_r^{-1} \boldsymbol{J}_r \boldsymbol{M}(\boldsymbol{\theta})^{-1} \boldsymbol{h}(\boldsymbol{\theta}, \dot{\boldsymbol{\theta}}, \phi) \tag{21}$$

where $X_r = \boldsymbol{J}_r \boldsymbol{M}(\boldsymbol{\theta})^{-1} \boldsymbol{J}_r^T$.

2.5 Numerical analysis of a virtual passive gait

Fig. 4 shows the simulation results of virtual passive walking where $\phi = 0.05$ [rad]. (a) is the stable limit cycle in phase plane, (b) is the trajectory w.r.t. time and (c) is the constraint force at the knee.

The walking cycle converges 1-periodic stable limit cycle as shown in (a). From (b), we can see that thigh and shank part of swing leg strike during swing stage and then the knee is locked and kept straight. The robot behaves like a compass robot. (c) is the constraint force at knee-joint which is used as knee torque after knee-strike.

In the next section, we will analyze its feature from a view point of control input by numerical simulations.

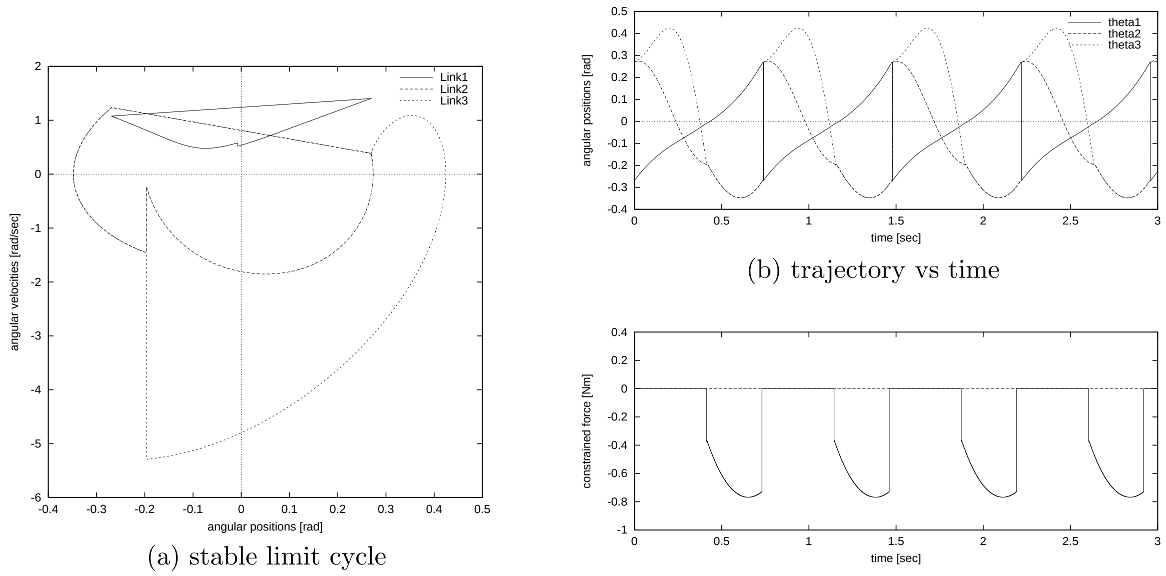

(a) stable limit cycle

(b) trajectory vs time

(c) constrained force vs time

Fig. 4. Simulation results of virtual passive walk($\phi = 0.05$ [rad])

2.6 Active walking

The dynamic equation of active walker with the constraint forces is expressed as

$$\boldsymbol{M}(\boldsymbol{\theta})\ddot{\boldsymbol{\theta}} + \boldsymbol{h}(\boldsymbol{\theta}, \dot{\boldsymbol{\theta}}) = -\boldsymbol{J}_r^T \lambda_r + \boldsymbol{\tau} + \boldsymbol{\tau}_e \tag{22}$$

where

$$\boldsymbol{h}(\boldsymbol{\theta}, \dot{\boldsymbol{\theta}}) = \boldsymbol{C}(\boldsymbol{\theta}, \dot{\boldsymbol{\theta}})\dot{\boldsymbol{\theta}} + \boldsymbol{g}(\boldsymbol{\theta}) \tag{23}$$

Here, please notice that the notations: $\boldsymbol{h}(\boldsymbol{\theta}, \dot{\boldsymbol{\theta}})$ denotes $\boldsymbol{h}(\boldsymbol{\theta}, \dot{\boldsymbol{\theta}}, 0)$ in Eq.(3) and $\boldsymbol{g}(\boldsymbol{\theta})$ denotes $\boldsymbol{g}(\boldsymbol{\theta}, 0)$ in Eq.(6) respectively.

We can tranceform the virtual gravity effect to actuator torque as shown in Fig. 5 which is given by

$$\boldsymbol{\tau} = \begin{bmatrix} (m_H l_1 + m_1 a_1 + m_2 l_1 + m_3 l_1)\cos\theta_1 \\ -(m_2 b_2 + m_3 l_2)\cos\theta_2 \\ -m_3 b_3 \cos\theta_3 \end{bmatrix} g \tan\phi \tag{24}$$

and from (7), we get

$$u_1 = ((m_H l_1 + m_1 a_1 + m_2 l_1 + m_3 l_1)\cos\theta_1 - (m_2 b_2 + m_3 l_2)\cos\theta_2)\, g \tan\phi \tag{25}$$

$$u_2 = ((m_2 b_2 + m_3 l_2)\cos\theta_2 + m_3 b_3 \cos\theta_3)\, g \tan\phi \tag{26}$$

$$u_3 = -m_3 b_3 \cos\theta_3 g \tan\phi. \tag{27}$$

Please notice that $\boldsymbol{\tau} = \boldsymbol{\tau}(\boldsymbol{\theta}, \phi)$ depends only on angular positions of the robot but does not depend on time. Since the control input is determined by only positional information, the control system is autonomous system.

Fig. 6 shows the simulated results of actuator torque vs time. The control is assumed to be implemented as a digitall controller, i.e., Z.O.H. is introduced in front of the actuator, where the control interval is 1.0 [msec]. We can see that the torque is almost constant. The constant-like torque is special feature of passive or virtual passive walking and it can be an indicator of "*natural motion*".

There are many algorithms which generate stable limit cycle on the floor. For example, INRIA proposed a method of energy-tracking control on a slope or floor[6]. It can generate steady walking pattern automatically without any gait design only by setting its target energy level. Though they titled "Passivity-mimicking control laws", the control law requires very large torque for each actuators in the case of walking on the floor. Utilizing the virtual gravity effect as in the proposed method, however, it has been checked that the small-torque walking can be realized and it requires less control input than that of INRIA's method.

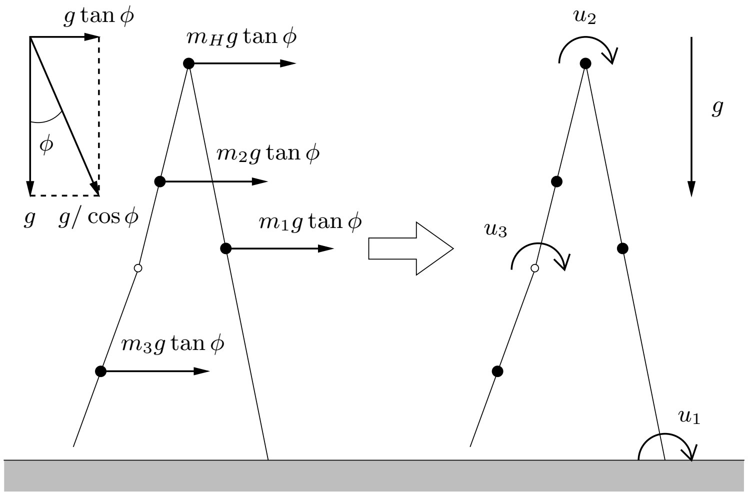

Fig. 5. Torque tranceformation

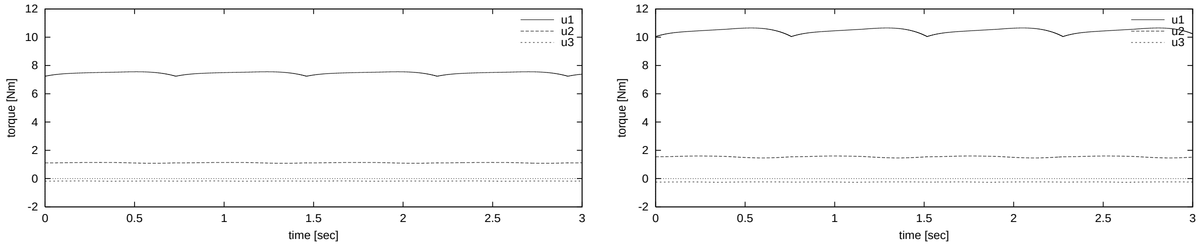

(a) $\phi = 0.05$ [rad]

(b) $\phi = 0.07$ [rad]

Fig. 6. Actuator torque vs time

3 Passive Velocity Field Control (PVFC)

3.1 Augmented mechanical system

In the basic PVFC the desired velocity field is time invariant, however, complex trajectories which has intersections can not be realized. "Self-pacing" which is an energy depending pseudo time is introduced[1], we will also use the virtual time.

The augmented coordinates is defined as $\boldsymbol{q} = \begin{bmatrix}\boldsymbol{\theta}^T & s & q_f\end{bmatrix}^T$. The dynamics of the flywheel and additional parameter are defined as

$$M_f \ddot{q}_f = \tau_f \tag{28}$$

$$\ddot{s} = \tau_s, \tag{29}$$

where q_f and s stand for angle of the flywheel and the virtual time, respectively. The augmented mechanical system is given by

$$\boldsymbol{M}^a(\boldsymbol{q})\ddot{\boldsymbol{q}} + \boldsymbol{C}^a(\boldsymbol{q},\dot{\boldsymbol{q}})\dot{\boldsymbol{q}} + \boldsymbol{g}^a(\boldsymbol{q}) = -\boldsymbol{J}_r^{aT}\lambda_r + \boldsymbol{\tau}^a + \boldsymbol{\tau}_e^a \tag{30}$$

where $\boldsymbol{\tau}^a$ is the augmented control force and $\boldsymbol{\tau}_e^a$ is the environmental forces. The details of matrices are defined as follows:

$$\boldsymbol{M}^a(\boldsymbol{q}) = \begin{bmatrix} \boldsymbol{M}(\boldsymbol{\theta}) & & \\ & 1 & \\ & & M_f \end{bmatrix},\quad \boldsymbol{C}^a(\boldsymbol{q},\dot{\boldsymbol{q}}) = \begin{bmatrix} \boldsymbol{C}(\boldsymbol{\theta},\dot{\boldsymbol{\theta}}) & & \\ & 0 & \\ & & 0 \end{bmatrix},\quad \boldsymbol{g}^a(\boldsymbol{q}) = \begin{bmatrix} \boldsymbol{g}(\boldsymbol{\theta}) \\ 0 \\ 0 \end{bmatrix},$$

$$\boldsymbol{J}_r^a = \begin{bmatrix} 0 \ -1 \ 1 \ 0 \ 0 \end{bmatrix},\quad \boldsymbol{\tau}^a = \begin{bmatrix} \boldsymbol{\tau} \\ \tau_s \\ \tau_f \end{bmatrix},\quad \boldsymbol{\tau}_e^a = \begin{bmatrix} \boldsymbol{\tau}_e \\ 0 \\ 0 \end{bmatrix}.$$

Please notice that the augmented mechanical system is decoupled system and PVFC makes coupling control input for the system.

3.2 Coupling control law

PVFC is considered to mechanical systems which do not have gravity term, so the gravity term should be canceled by control forces. Then let the control forces reformed as:

$$\boldsymbol{\tau}^a = \bar{\boldsymbol{\tau}}^a + \boldsymbol{g}^a(\boldsymbol{q}) \tag{31}$$

where $\bar{\boldsymbol{\tau}}_a$ is virtual control input. Then the dynamics of the robot system can be rewritten

$$\boldsymbol{M}^a(\boldsymbol{q})\ddot{\boldsymbol{q}} + \boldsymbol{C}^a(\boldsymbol{q},\dot{\boldsymbol{q}})\dot{\boldsymbol{q}} = \bar{\boldsymbol{\tau}}^a + \boldsymbol{\tau}_e^a. \tag{32}$$

For this system, we can apply PVFC for the system.

The coupling control $\bar{\boldsymbol{\tau}}^a$ in (32) is given by

$$\bar{\boldsymbol{\tau}}_a = \boldsymbol{G}(\boldsymbol{q},\dot{\boldsymbol{q}})\dot{\boldsymbol{q}} + \gamma\boldsymbol{R}(\boldsymbol{q},\dot{\boldsymbol{q}})\dot{\boldsymbol{q}} \tag{33}$$

where $\boldsymbol{G}$ is feed-forward term and $\boldsymbol{R}$ is feedback term, both of them are skew-symmetric. γ is the feedback gain. The details are as follows:

$$\boldsymbol{G}(\boldsymbol{q},\dot{\boldsymbol{q}}) = \frac{\boldsymbol{\varDelta}\boldsymbol{Q}^T - \boldsymbol{Q}\boldsymbol{\varDelta}^T}{\boldsymbol{Q}^T\boldsymbol{V}_a} \tag{34}$$

$$\boldsymbol{R}(\boldsymbol{q},\dot{\boldsymbol{q}}) = \boldsymbol{Q}\boldsymbol{p}^T - \boldsymbol{p}\boldsymbol{Q}^T \tag{35}$$

where

$$\boldsymbol{p}(\boldsymbol{q},\dot{\boldsymbol{q}}) = \boldsymbol{M}^a(\boldsymbol{q})\dot{\boldsymbol{q}} \tag{36}$$

$$\boldsymbol{Q}(\boldsymbol{q}) = \boldsymbol{M}^a(\boldsymbol{q})\boldsymbol{V}_a(\boldsymbol{q}) \tag{37}$$

$$\boldsymbol{\varDelta}(\boldsymbol{q},\dot{\boldsymbol{q}}) = \boldsymbol{M}^a(\boldsymbol{q})\frac{d}{dt}\boldsymbol{V}_a(\boldsymbol{q}) + \boldsymbol{C}^a(\boldsymbol{q},\dot{\boldsymbol{q}})\boldsymbol{V}_a(\boldsymbol{q}) \tag{38}$$

When external forces are absent, (i.e., $\boldsymbol{\tau}_e = \boldsymbol{0}$), the passive velocity field controller will achieve $\dot{\boldsymbol{q}} \to \beta\boldsymbol{V}_a$ where β is given by

$$\beta = \sqrt{\frac{\dot{\boldsymbol{q}}^T\boldsymbol{M}^a(\boldsymbol{q})\dot{\boldsymbol{q}}}{\boldsymbol{V}_a^T\boldsymbol{M}^a(\boldsymbol{q})\boldsymbol{V}_a}}. \tag{39}$$

Please see [1] in detail.

3.3 Properties of PVFC

Differentiating K^a w.r.t. time, and substituting (32),

$$\frac{d}{dt}K^a(\boldsymbol{q},\dot{\boldsymbol{q}}) = \frac{d}{dt}\left(\frac{1}{2}\dot{\boldsymbol{q}}^T\boldsymbol{M}(\boldsymbol{q})\dot{\boldsymbol{q}}\right) = \dot{\boldsymbol{q}}^T\boldsymbol{\tau}_e^a = \dot{\boldsymbol{\theta}}^T\boldsymbol{\tau}_e. \tag{40}$$

Hence, using K^a as the storage function, the feedback system is shown to be passive.

4 Velocity Field Design

4.1 Approximation of a limit cycle

The stable limit cycle can be approximated by RBF (Radial Basis Function). Though there are several methods to approximate functions, we use RBF since it can be calculated effectively and the determination of the weights is easy. The desired trajectory $\boldsymbol{\theta}_d$ is represented by

$$\boldsymbol{\theta}_d(s) = \begin{bmatrix} \theta_{d1}(s) \\ \theta_{d2}(s) \\ \theta_{d3}(s) \end{bmatrix} = \sum_{i=1}^{N} \boldsymbol{w}_i \phi(s, s_i) \tag{41}$$

$$\phi(s, s_i) = \exp\left(-\frac{(s - s_i)^2}{2\sigma^2}\right), \tag{42}$$

$$\boldsymbol{w}_i = \begin{bmatrix} w_{1i} \; w_{2i} \; w_{3i} \end{bmatrix}^T . \tag{43}$$

The weight $\boldsymbol{w}_i$ can be obtained by the least square approximation. If $\boldsymbol{\Phi}, \boldsymbol{\Gamma}$ and $\boldsymbol{w}$ are defined as

$$\boldsymbol{\Phi} = \begin{bmatrix} \phi(s_1, s_1) & \phi(s_1, s_2) & \cdots & \phi(s_1, s_N) \\ \phi(s_2, s_1) & \phi(s_2, s_2) & \cdots & \phi(s_2, s_N) \\ \vdots & \vdots & \ddots & \vdots \\ \phi(s_N, s_1) & \phi(s_N, s_2) & \cdots & \phi(s_N, s_N) \end{bmatrix}, \quad \boldsymbol{\Gamma} = \begin{bmatrix} \boldsymbol{\theta}_{d1}^T \\ \boldsymbol{\theta}_{d2}^T \\ \vdots \\ \boldsymbol{\theta}_{dN}^T \end{bmatrix}, \quad \boldsymbol{w} = \begin{bmatrix} \boldsymbol{w}_1^T \\ \boldsymbol{w}_2^T \\ \vdots \\ \boldsymbol{w}_N^T \end{bmatrix}, \tag{44}$$

$\boldsymbol{w}$ is given by $\boldsymbol{w} = \boldsymbol{\Phi}^{-1}\boldsymbol{\Gamma}$ since the relation $\boldsymbol{\Phi}\boldsymbol{w} = \boldsymbol{\Gamma}$ should hold, The number of data N is chosen empirically in this paper. Fig. 7 shows the data of desired trajectory and Fig. 8 shows its fitting results.

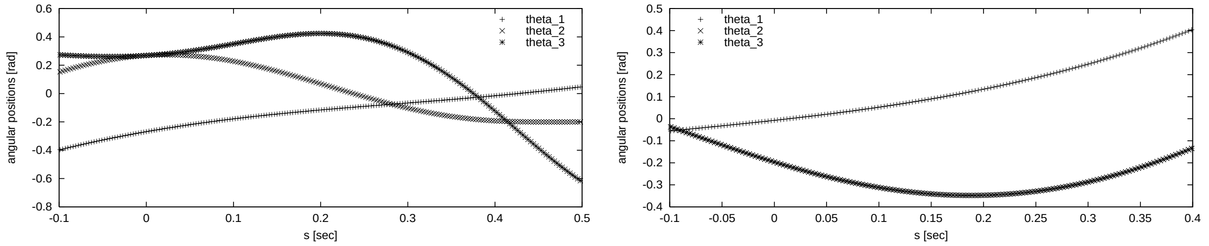

(a) phase 1 ($N = 200$) (b) phase 2 ($N = 167$)

Fig. 7. Data of desired trajectory

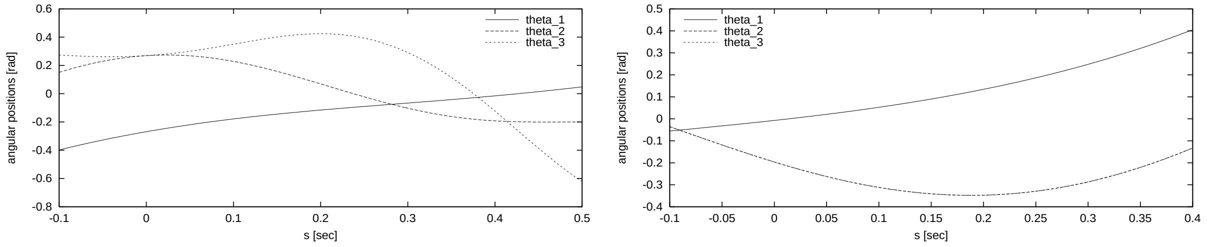

(a) phase 1 ($\sigma = 0.0065$) (b) phase 2 ($\sigma = 0.0068$)

Fig. 8. Fitting results

4.2 Desired velocity field of the original system

The velocity field of original system is defined as follows:

$$\boldsymbol{V}(\boldsymbol{\theta}, s) = \begin{bmatrix} \begin{bmatrix} V_1 \\ V_2 \\ V_3 \end{bmatrix} \\ V_s \end{bmatrix} = \lambda_1(\boldsymbol{\theta}, s) \begin{bmatrix} \frac{\partial}{\partial s}\boldsymbol{\theta}_d(s) \\ 1 \end{bmatrix} - \lambda_2(\boldsymbol{\theta}, s) \begin{bmatrix} \boldsymbol{\theta}(t) - \boldsymbol{\theta}_d(s) \\ 0 \end{bmatrix} \tag{45}$$

$$\lambda_1(\boldsymbol{\theta}, s) = \exp\left(-R\|\boldsymbol{\theta}(t) - \boldsymbol{\theta}_d(s)\|\right) \tag{46}$$

$$\lambda_2(\boldsymbol{\theta}, s) = 2.0 - \exp\left(-R\|\boldsymbol{\theta}(t) - \boldsymbol{\theta}_d(s)\|\right) \tag{47}$$

where $R > 0$. Therefore, when tracking error is large, the desired trajectory $\boldsymbol{\theta}_d$ progresses at a slower speed. This approach will be referred to as “self pacing”.

4.3 Augmented velocity field

The total kinetic energy of the augmented system evaluated at the desired velocity field $\boldsymbol{V}(\boldsymbol{q})$ is constant, i.e. in local coordinates the following condition is satisfied for all $\boldsymbol{q}$:

$$K^a(\boldsymbol{q}, \boldsymbol{V}_a(\boldsymbol{q})) = \frac{1}{2}\boldsymbol{V}_a^T(\boldsymbol{q})\boldsymbol{M}^a(\boldsymbol{q})\boldsymbol{V}_a(\boldsymbol{q}) = K_d^a > 0 \tag{48}$$

where K_d^a is a positive scalar and $\boldsymbol{V}_a(\boldsymbol{q})$ is of the form

$$\boldsymbol{V}_a(\boldsymbol{q}) = \left[\boldsymbol{V}^T(\boldsymbol{\theta}, s)\; V_f(\boldsymbol{\theta}, s)\right]^T. \tag{49}$$

Above condition implies that $\boldsymbol{V}_a(\boldsymbol{q})$ can be defined by specifying K_d^a in the first and then by determining the desired velocity field for the fictitious inertia $V_f(\boldsymbol{\theta})$ in (49) using

$$V_f(\boldsymbol{\theta}, s) = \sqrt{\frac{2}{M_f}\left(K_d^a - K(\boldsymbol{\theta}, s)\right)}, \tag{50}$$

where K is kinetic energy of the original system. Then the kinetic energy of the augmented system is kept constant value. In this paper, we set the parameters as shown in Table 2.

4.4 Numerical Simulations

Fig. 9 shows the simulation results where the controller assumed to be implemented as a digital control and the control interval is 1.0 [msec]. The simulation conditions are all the same for the following simulations. Since the computing of $d\boldsymbol{V}_a(\boldsymbol{q})/dt$ requires heavy tasks, it is computed by $\Delta\boldsymbol{V}_a(\boldsymbol{q})/\Delta t$ approximately.

We set initial velocities of the additional parameters as $\dot{s}(0) = 1.0$ [m/sec] and $\dot{q}_f = 1.5$ [m/sec]. In this case, $K^a(0) = 20.5215$ [J] and we set $K_d^a = K^a(0)$.

Since the robot is forced by reaction force from the floor at every heel-strike instant, kinetic energy of the robot dissipates at every step. (At knee-strike instant it also dissipates) This implies that kinetic energy of the augmented mechanical system also dissipates at every step. So the walking speed becomes slower according to PVFC. (a) is the phase plane trajectory of stance leg. The cycle is going to clash along only velocity direction. This implies that the walking pattern does not change any even if the walking speed changes. (b) shows the angular positions vs time. We can see that the motion does not change but step period becomes longer. (c) shows the kinetic energy vs time. All kinetic energy dissipates at every transition instant but kinetic energy is kept constant during single support phase according to PVFC.

Above phenomena occurs because the control plant is hybrid system which contains collisions and has uncontinuous changes of velocities of the system. Then we must consider some reset algorithms for post-impact velocities of the additional parameters.

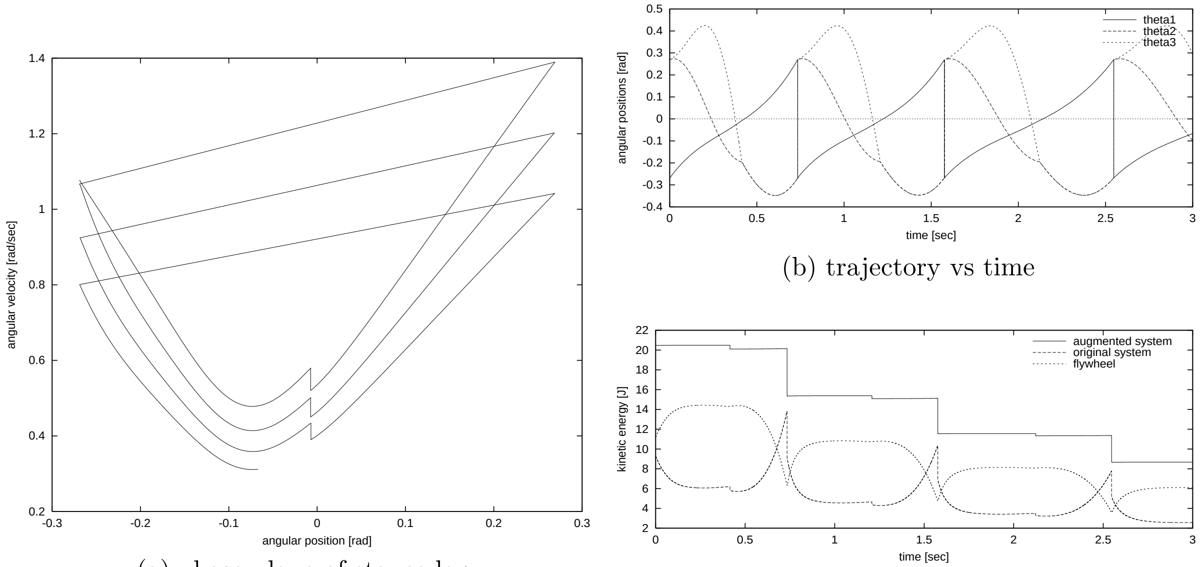

(b) trajectory vs time

(a) phase plane of stance leg

(c) kinetic energy vs time

Fig. 9. Simulation results in the case without reset

5 Reset and switching algorithm for variable constrained mechanical system

5.1 Switching control

Since the knee torque is not required after knee-lock, the control is switched at knee-strike instant. The control algorithm is formed as follows:

1. Before the knee-lock: full-control of PVFC is used as given by

$$\boldsymbol{\tau} = \begin{bmatrix} 1 & 1 & 0 \\ 0 & -1 & -1 \\ 0 & 0 & 1 \end{bmatrix} \begin{bmatrix} u_1 \\ u_2 \\ u_3 \end{bmatrix}, \tag{51}$$

$$\lambda_r = 0. \tag{52}$$

2. After the knee-lock: the control input to knee-joint of swing leg is cut off and the knee-joint is mechanically locked and kept straight after knee-strike as

$$\boldsymbol{\tau} = \begin{bmatrix} 1 & 1 \\ 0 & -1 \\ 0 & 0 \end{bmatrix} \begin{bmatrix} u_1 \\ u_2 \end{bmatrix}, \tag{53}$$

$$\boldsymbol{J}_r^T \lambda_r = \begin{bmatrix} 0 \\ -1 \\ 1 \end{bmatrix} \left(-X_r^{-1} \boldsymbol{J}_r \boldsymbol{M}(\boldsymbol{\theta})^{-1} \boldsymbol{h}(\boldsymbol{\theta}, \dot{\boldsymbol{\theta}}) \right). \tag{54}$$

5.2 Reset algorithm of initial velocity of the flywheel

Since kinetic energy of the robot dissipates at every collision instant, that of the augmented mechanical system also dissipates at every collision instant. In order to realize steady walking by PVFC, we must recover kinetic energy of the augmented mechanical system by some algorithms. One of the method is as follows.

Kinetic energy of the augmented system K^a, that of the original system K and that of the flywheel K_f are given by:

$$K^a = K + K_f \tag{55}$$

$$K = \frac{1}{2}\dot{\boldsymbol{\theta}}^T \boldsymbol{M}(\boldsymbol{\theta})\dot{\boldsymbol{\theta}} + \frac{1}{2}\dot{s}^2 \tag{56}$$

$$K_f = \frac{1}{2}M_f\dot{q}_f^2. \tag{57}$$

From above equations, post-impact velocity of the flywheel $\dot{q}_f$ is reset as

$$\dot{q}_f^+ = \sqrt{\frac{2}{M_f}\left(K_d^a - K^+\right)} \tag{58}$$

where it can be considered that an appropriate impulsive force is applied for the flywheel. Then we can recover and keep K^a constant value during every single support phase if $\boldsymbol{\tau}_e^a = \mathbf{0}$.

Table 2. Reset algorithm for additional parameters

	Phase 1	Phase 2
$\dot{q}_f$ reset	See (58)	See (58)
q_f reset	—	—
$\dot{s}$ reset	—	—
s reset	0.0 [m]	0.0 [m]
$K_d^a(\boldsymbol{q}, \dot{\boldsymbol{q}})$ settings	$K^a(0)$ [J]	$K^a(0)$ [J]

5.3 Numerical Simulations

If the walking robot was pushed toward the walking direction, the walking speed should increase because energy of the augmented system increases according to PVFC. We examined the effect of such environmental forces.

Fig. 10 and 11 shows the simulation results and the difference of the condition is only the external force, i.e., 13 [N] for Fig. 10 and 20 [N] for Fig. 11. Furthermore, we consider the input saturation given by

$$|u_i| \leq 20.0 \quad (i = 1, 2, 3) \tag{59}$$

for the implementation.

First, the robot exhibits steady walking by the reset of initial velocity of the flywheel and it is pushed toward the horizontal direction just after fast-impact instant during 0.3 [sec]. Conserving post-pushing energy of the augmented system as $K_d^a(\boldsymbol{q}, \dot{\boldsymbol{q}})$, the walking motion slide to fast-steady walking pattern.

From (a) and (b), we can see that the trajectory of stance leg is going to sliding only along velocity direction. This implies that the walking pattern does not change even if the walking speed changes. From (c) and (e), it can be seen that the kinetic energy increases after pushing by β times. From (d), we can see that the control torque becomes inconstant after pushing. This implies that the control torque becomes unsuitable for *natural* virtual passive motion in high-speed walking. Based on the observation, we introduce "multi-pattern walking" in the next section.

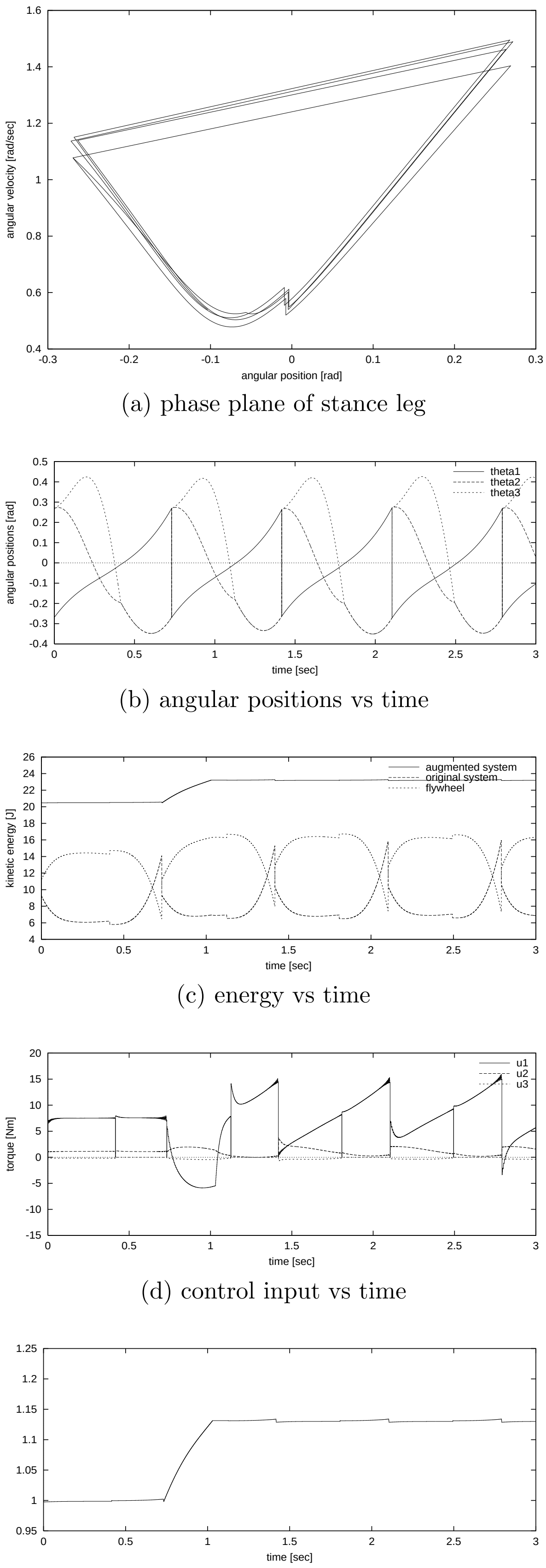

(a) phase plane of stance leg

(b) angular positions vs time

(c) energy vs time

(d) control input vs time

(e) β vs time

Fig. 10. Simulation result (13.0 [N])

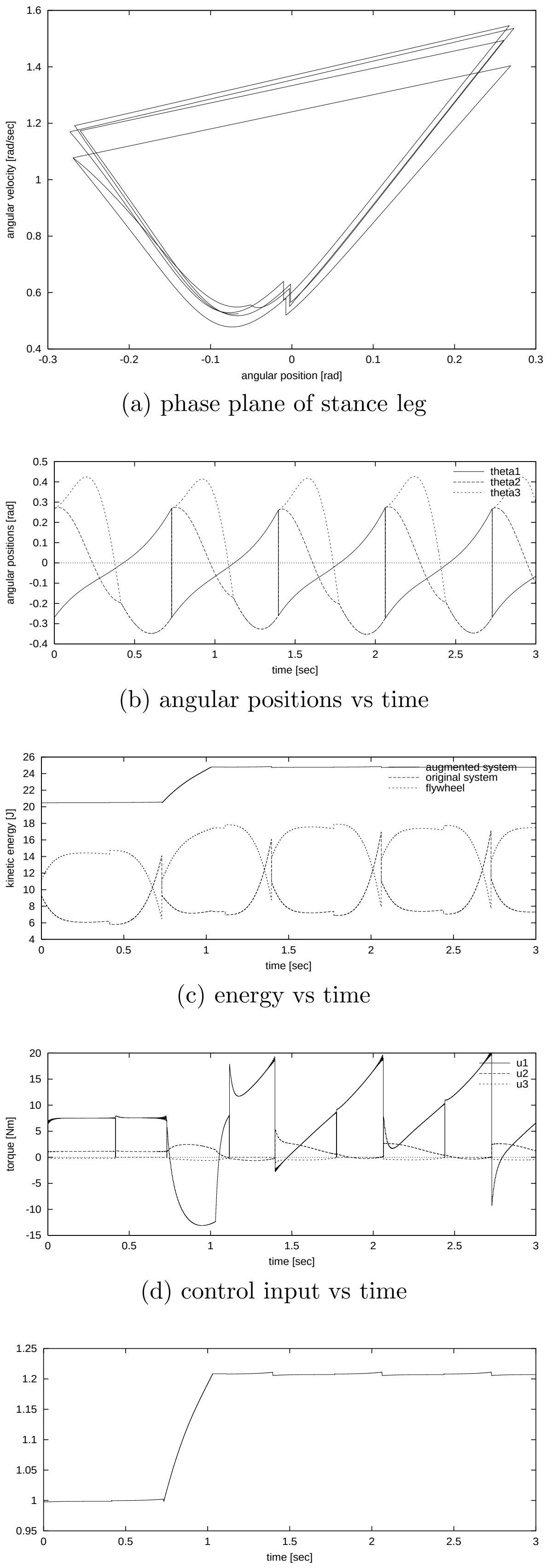

(a) phase plane of stance leg

(b) angular positions vs time

(c) energy vs time

(d) control input vs time

(e) β vs time

Fig. 11. Simulation results (20.0 [N])

6 Extended PVFC and Multi-pattern Walking

6.1 Multi-pattern walking

In the previous section we have seen that the control torque becomes unsuitable for robot dynamics from a viewpoint of constant-like torque in virtual passive walking.

Based on the observation, the walking motion should be modified according to its energy level because one energy level has its own stable limit cycle and its tracking speed. In this section, we will combine two walking patterns, fast motion and slow motion. The fast motion is obtained in more inclined slope and we set the slow motion as previous motion ($\phi = 0.05$ [rad]).

6.2 Velocity field design

In order to change the velocity field w.r.t. its energy levels, we must use the information of β in design of desired velocity field $\boldsymbol{V}_a$ because it is a proportion of energy level to the nominal level. If we use it, however, there occurs a problem of acceleration feedback in Eq.(38) because

$$\frac{d}{dt}\boldsymbol{V}_a(\boldsymbol{q},\beta) = \frac{\partial \boldsymbol{V}_a(\boldsymbol{q},\beta)}{\partial \boldsymbol{q}}\dot{\boldsymbol{q}} + \frac{\partial \boldsymbol{V}_a(\boldsymbol{q},\beta)}{\partial \beta}\dot{\beta} = \dot{\boldsymbol{V}}_a(\boldsymbol{q},\dot{\boldsymbol{q}},\ddot{\boldsymbol{q}}) \tag{60}$$

and this implies that $\varDelta(\boldsymbol{q},\dot{\boldsymbol{q}},\ddot{\boldsymbol{q}})$ and $\bar{\boldsymbol{\tau}}^a(\boldsymbol{q},\dot{\boldsymbol{q}},\ddot{\boldsymbol{q}})$. In order to avoid the direct feedback which may destroy the well-posedness of the system, we introduce estimation of β in virtual time. In order to design the estimator, we assume

$$\frac{d\beta}{ds} = \dot{\beta}\frac{dt}{ds} = 0 \tag{61}$$

$$\dot{s} = \beta V_s. \tag{62}$$

This implies that $\dot{\beta} = 0$ for $dt/ds \neq 0$. If we consider that β and $\dot{s}$ are state and output respectively, an observer for β is given by

$$\frac{d\hat{\beta}}{ds} = -\frac{L}{V_s}(\dot{s} - V_s\hat{\beta}) \tag{63}$$

where $L < 0$ is a scalar, and $\hat{\beta} \to \beta$ is achieved if $ds/dt > 0$. Please notice that $\hat{\beta}$ just depends on s which is one of the state of the augmented system, and using the estimated β and $\hat{\beta}$, the following relationship is maintained:

$$\frac{d}{dt}\boldsymbol{V}_a(\boldsymbol{q},\hat{\beta}) = \frac{\partial \boldsymbol{V}_a(\boldsymbol{q},\hat{\beta})}{\partial \boldsymbol{q}}\dot{\boldsymbol{q}} = \dot{\boldsymbol{V}}_a(\boldsymbol{q},\dot{\boldsymbol{q}}), \tag{64}$$

due to Eq.(63).

Next, the two walking pattern are combined in convex-like form as:

$$\boldsymbol{\theta}_d(s,\zeta) = (1-\zeta)\boldsymbol{\theta}_{dS}(s) + \zeta\boldsymbol{\theta}_{dF}(s) \tag{65}$$

where $\boldsymbol{\theta}_{dS}$ is the desired trajectory of slow motion ($\phi = 0.05$ [rad]) and $\boldsymbol{\theta}_{dF}$ is that of fast motion ($\phi = 0.07$ [rad]). ζ is defined by:

$$\zeta(\hat{\beta}) = \frac{1}{1 + \exp\left(-\xi_1\left(\hat{\beta} - \beta_1^*\right)\right)} \tag{66}$$

So in the case with high-energy level, the motion slides $\boldsymbol{\theta}_{dF}$ because of $\zeta \to 1.0$.

Next, let us consider desired velocity filed. By only differentiating with s, the desired tracking speed V_s does not change suitably with natural virtual walking motion. Therefore, we must divide desired velocity field with some gains. The desired velocity of the robot is determined as follows:

$$\boldsymbol{v}_d(s,\zeta,\eta) = \frac{1}{\eta}\frac{\partial \boldsymbol{\theta}_d(s)}{\partial s} \tag{67}$$

where $\eta(\zeta)$ is modulated gain defined as:

$$\eta(\zeta) = 1.0 + \zeta(\beta_2^* - 1.0) \quad (0 < \zeta < 1) \tag{68}$$

Then from above equations, the desired velocity field of the original system can be formulated as:

$$\boldsymbol{V}(\boldsymbol{\theta}, s) = \begin{bmatrix} \begin{bmatrix} V_1 \\ V_2 \\ V_3 \end{bmatrix} \\ V_s \end{bmatrix} = \lambda_1(\boldsymbol{\theta}, s) \begin{bmatrix} \boldsymbol{v}_d(s, \eta) \\ \eta^{-1} \end{bmatrix} - \lambda_2(\boldsymbol{\theta}, s) \begin{bmatrix} \boldsymbol{\theta}(t) - \boldsymbol{\theta}_d(s) \\ 0 \end{bmatrix} \tag{69}$$

The tuning parameter β_1^* and β_2^* should be determined by some algorithms. One method is, for example, divide K_d^a of fast single motion with that of slow motion; that is,

$$\beta_2^* = \frac{K_d^a(\phi = 0.07)}{K_d^a(\phi = 0.05)} = 1.0625 \tag{70}$$

Then we are also able to determine $\beta_1^* = 1.03125$ which is center value between 1.0 and β_2^*, that is,

$$\beta_1^* = \frac{1.0 + \beta_2^*}{2.0} = 1.03125. \tag{71}$$

If we want to make the control system more sensitive to the pushing force, β_1^* and β_2^* should be set smaller value. In that case, the walking motion should change with small force because $K^a(\boldsymbol{q}, \dot{\boldsymbol{q}})$ increases more sensitively.

Table 3. Tuning parameters

Parameters	Slow motion	Middle motion	Fast motion
ζ	0.0	0.5	1.0
η	1.0	β_1^*	β_2^*

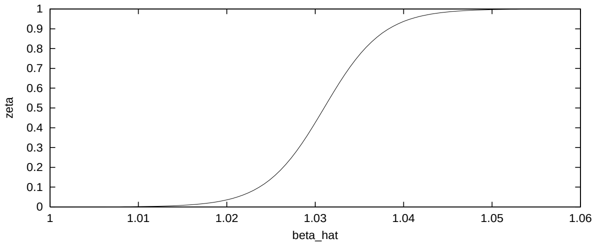

Fig. 12. ζ vs $\hat{\beta}$ ($\xi_1 = 300.0$)

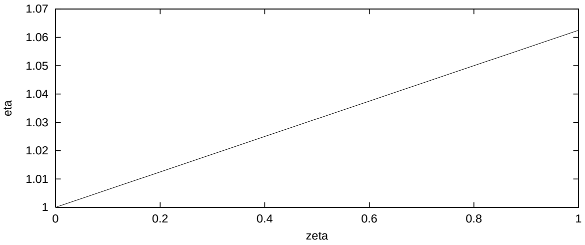

Fig. 13. η vs ζ ($\xi_2 = 10.0$)

6.3 Numerical simulations

Fig. 14 and 15 shows the simulation results where the the all simulated situations are identical with the previous ones. In this section, we also examined the effect of environmental forces.

Conserving post-pushing energy of the augmented system as $K_d^a(\boldsymbol{q}, \dot{\boldsymbol{q}})$, the walking motion slides and converges to fast-*natural* virtual passive walking pattern where $\phi = 0.07$ [rad].

From (a) and (b) in each case, we can see that the trajectory of stance leg is going to slide and converge new walking pattern which is *natural* virtual passive gait where $\phi = 0.07$ [rad]. From (d) in Fig. 14, it is clear that the control torque changes from constant-like torque to new level of the similar after pushing. This implies that the motion slides from natural one to natural another. With more pushing force, Fig. 15 (d), we can see that the change of the control torque becomes smaller than that of Fig. 11 (d). (e) shows the control parameters in the simulation. In Fig. 14, it can be seen that $\eta \to \beta_2^*$ and other parameters converge nominal values. In Fig. 15, β converges a larger value because of larger force than that in Fig. 14, however, η does not change any more. So the walking pattern also does not change any more though the modulation of the control input becomes slightly big.

From above results and observations, it is checked that more natural walking has been realized by multi-desired velocity field.

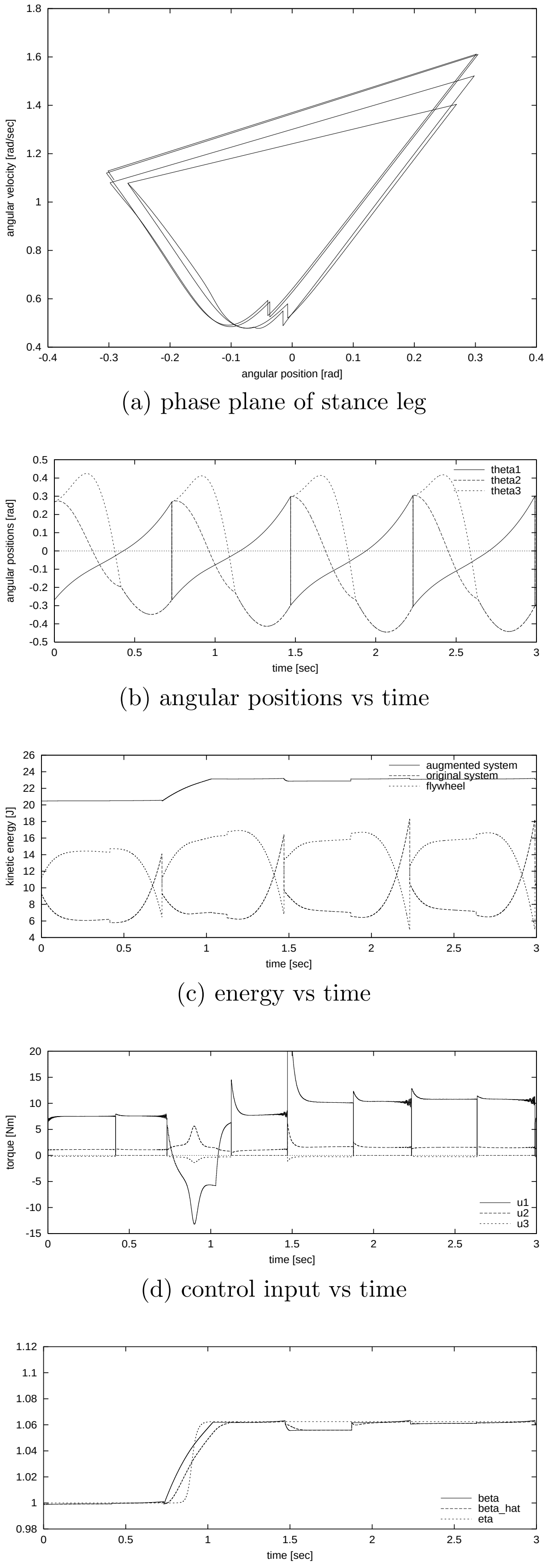

(a) phase plane of stance leg

(b) angular positions vs time

(c) energy vs time

(d) control input vs time

(e) $\beta, \hat{\beta}, \eta$ vs time

Fig. 14. Simulation results (13.0 [N])

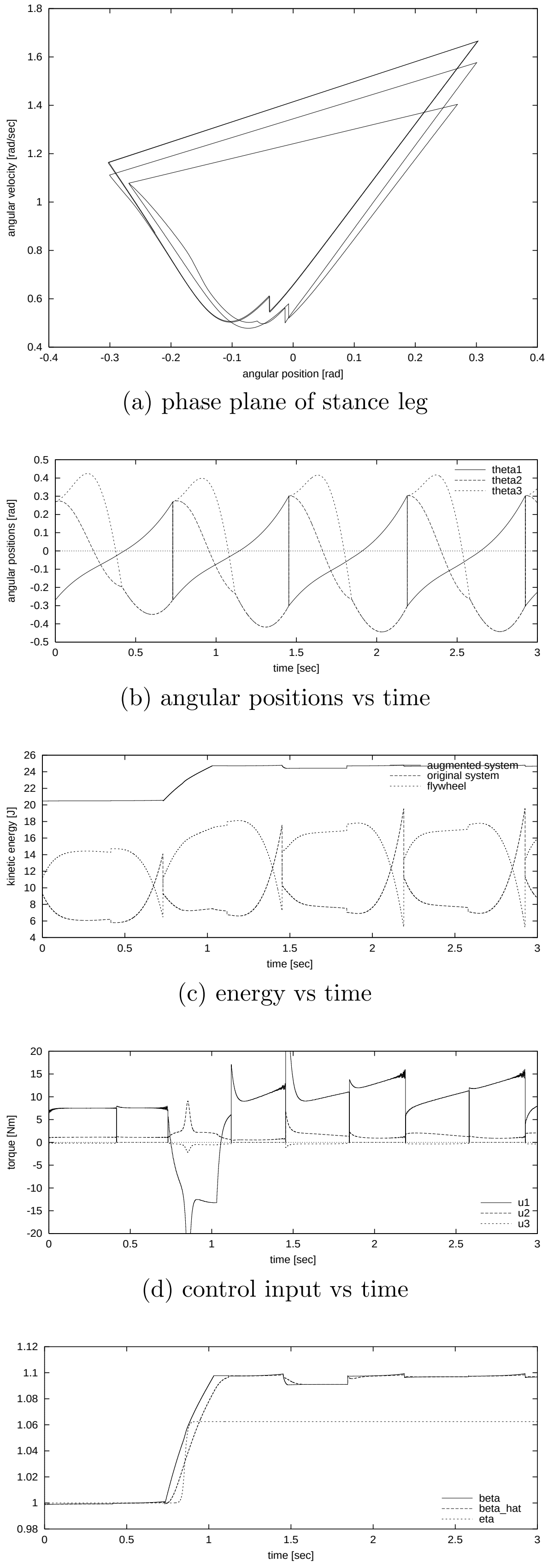

(a) phase plane of stance leg

(b) angular positions vs time

(c) energy vs time

(d) control input vs time

(e) $\beta, \hat{\beta}, \eta$ vs time

Fig. 15. Simulation results (20.0 [Nm])

6.4 Extrapolation of the desired velocity fields

In previous section, we have considered "*interpolation*" method. Next we consider "*affine*" method to realize more constant-like and smooth control input. The formulation of 6.2 (case1) can make suitable control input only in the duration $1.0 \le \eta \le \beta_2^*$, however, extending the duration of ζ better control performance will be obtained. Let us refine ζ as

$$\zeta(\hat{\beta}) = \frac{K}{1 + \exp\left(-\xi_1\left(\hat{\beta} - \beta_1^*\right)\right)} \tag{72}$$

where K is tuning parameter then $0 \le \zeta \le K$. We consider 3 cases shown in Table 4. Fig. 16 shows ζ vs $\hat{\beta}$. In all case, $\zeta(\hat{\beta})$ pass through the point near $(\zeta, \hat{\beta}) = (1.0, \beta_2^*)$. Fig. 17 and 18 shows the simulation results Fig. 10 and 11 shows the simulation results where the all simulated situations are identical with Fig. 15. Please see Fig. 15 for the results of case1. From Fig. 17 and 18 we can see the validity of proposed method and the case2 gives better performance than that of case1 as expected. The more analysis is left in the future work.

Table 4. Tuning parameters

	β_1^*	ξ_1	K
case1	1.03125	300	1.0
case2	1.045	150	1.1
case3	1.050	160	1.2

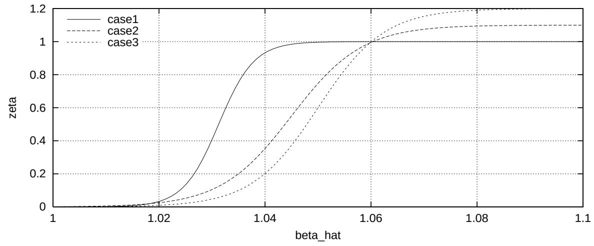

Fig. 16. ζ vs $\hat{\beta}$

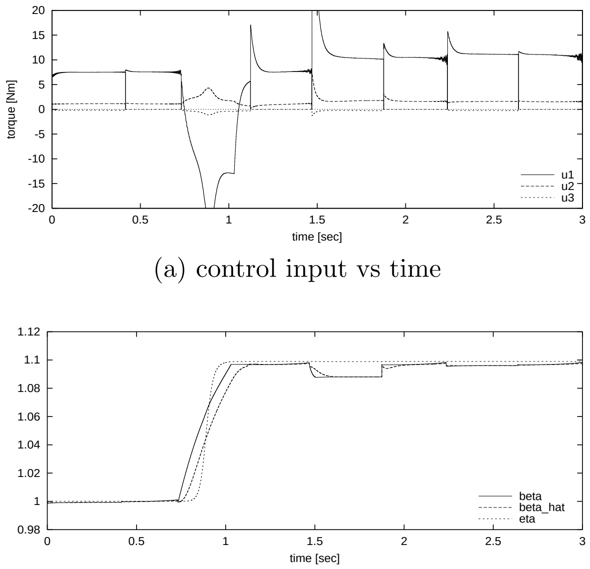

(a) control input vs time

(b) $\beta, \hat{\beta}, \eta$ vs time

Fig. 17. Simulation results (case1)

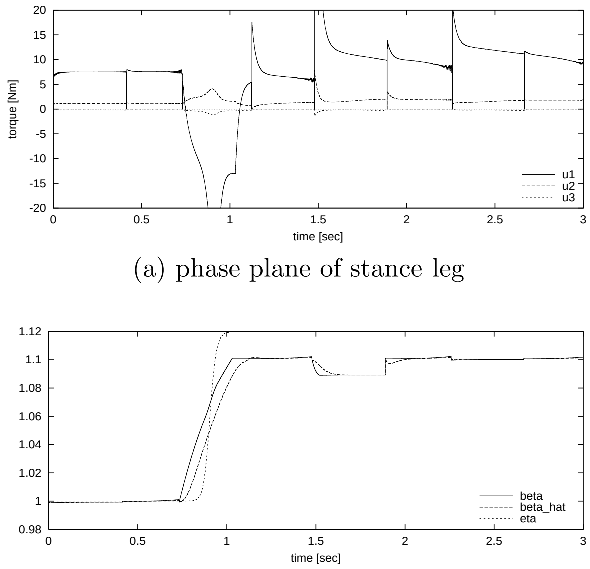

(a) phase plane of stance leg

(b) $\beta, \hat{\beta}, \eta$ vs time

Fig. 18. Simulation results (case2)

7 Conclusions

In this paper, we proposed a method to apply an extended PVFC with multi velocity field to a biped walking robot which has knee-joints and the validity of control law have numerically examined by computer simulations. With the control method the walking robot interacts with its physical environment in an energetically passive manner because of passivity of the control system, and we can change its walking speed easily by modifying a virtual energy. We introduced multi-pattern walking for more natural walk using multi desired velocity field. According to this method, the walking motion can slide from slow motion to fast motion and the motion becomes a natural virtual passive gait. A method to compensate for the energy loss at walking phases due to collisions to the floor was also proposed and steady walking was realized.

References

1. Perry Y. Li and R. Horowitz, "Passive Velocity Field Control of Mechanical Manipulators," *Trans. on Roboticrs and Automation*, Vol. 15, No. 4, pp. 751-763, 1999.
2. Perry Y. Li and R. Horowitz, "Passive Velocity Field Control Approach to Robot Contour Following," *Proc. of the Japan/USA Symposium on Flexible Automation*, Vol. 1, pp. 25-32, 1996.
3. M.Yamakita et. al, "Decentralized Cooperative Controller for Multiple Robotic Systems Based on Passive Velocity Field Control," *Proc. of ISIAC'98*, 1998.
4. M.Yamakita et. al, "An Application of Passive Velocity Field Control to Cooperative multiple 3-Wheeled Mobile Robots," *Proc. of IROS'98*, Vol. 1, pp. 368-373, 1998.
5. A. Goswami, B. Espiau and A. Keramane, "Compass-like Biped Robot Part I: Stability and Bifurcation of Passive Gaits," *Research report INRIA*, No. 2613, 1996.
6. A. Goswami, B. Espiau and A. Keramane, "Limit Cycles in a Passive Compass Gait Biped and Passivity-Mimicking Control Laws," j*Autonomous Robots*, Vol. 4, No. 3, pp. 273-286, 1997.
7. A. Goswami, B. Thuilot and B. Espiau, "A Study of the Passive Gait of a Compass-Like Biped Robot: Symmetry and Chaos," *The Int. J. of Robotics Research*, Vol. 17, No. 12, pp. 1282-1301, 1998.
8. T. McGeer, "Passive dynamic walking," *The Int. J. of Robotics Research*, Vol. 9, pp. 62-82, 1990.
9. M. Garcia, et. al., "The Simplest Walking Model: Stability, Complexity, and Scaling," *ASME J. of Biomechanical Engineering*, Vol. 120, pp. 281-288, 1998.
10. M. Garcia, A. Chatterjee and A. Ruina, "Speed, Efficiency, and Stability of Small-Slope 2-D Passive Dynamic Bipedal Walking," *Int. Conf. on Robotics and Automation*, pp. 2351-2356, 1998.
11. M. Yamakita, F. Asano and K. Furuta, "Passive Velocity Field Control of Biped Walking Robot," *Int. Conf. on Robotics and Automation*, Vol. 3, pp. 3057-3062, 2000.
12. F. Asano, M. Yamakita and K. Furuta, "Stabilizing control of passive biped robot and its application to active walking," *Proc. of AROB 5th'00*, Vol. 2, pp. 503-506, 2000.
13. M. W. Spong, "Passivity based control of the compass gait biped," *14th World Congress of IFAC*, 1999.
14. G. W. Howell and J. Baillieul, "Simple controllable walking mechanisms which exhibit bifurcations," *The 37th IEEE Conf. on Decision and Control*, pp. 3027-3032, 1998.